



HAL
open science

Fluctuation-induced quantum friction in nanoscale water flows

Nikita Kavokine, Marie-Laure Bocquet, Lydéric Bocquet

► **To cite this version:**

Nikita Kavokine, Marie-Laure Bocquet, Lydéric Bocquet. Fluctuation-induced quantum friction in nanoscale water flows. *Nature*, 2022, 602, pp.84-90. 10.1038/s41586-021-04284-7 . hal-03388180

HAL Id: hal-03388180

<https://hal.science/hal-03388180>

Submitted on 4 Oct 2022

HAL is a multi-disciplinary open access archive for the deposit and dissemination of scientific research documents, whether they are published or not. The documents may come from teaching and research institutions in France or abroad, or from public or private research centers.

L'archive ouverte pluridisciplinaire **HAL**, est destinée au dépôt et à la diffusion de documents scientifiques de niveau recherche, publiés ou non, émanant des établissements d'enseignement et de recherche français ou étrangers, des laboratoires publics ou privés.

Fluctuation-induced quantum friction in nanoscale water flows

Nikita Kavokine^{1,2,*}, Marie-Laure Bocquet³ and Lydéric Bocquet^{1*}

¹*Laboratoire de Physique de l'École Normale Supérieure,
ENS, Université PSL, CNRS, Sorbonne Université,*

Université Paris-Diderot, Sorbonne Paris Cité, Paris, France

²*Center for Computational Quantum Physics, Flatiron Institute,
162 5th Avenue, New York, NY 10010, USA and*

³*PASTEUR, Département de Chimie, École Normale Supérieure, PSL University,
Sorbonne Universités, CNRS, 24 Rue Lhomond, 75005, Paris, France*

The flow of water in carbon nanochannels has defied understanding thus far [1], with accumulating experimental evidence for ultra-low friction, exceptionally high water flow rates, and curvature-dependent hydrodynamic slippage [2–5]. In particular, the mechanism of water-carbon friction remains unknown [6], with neither current theories [7], nor classical [8, 9] or *ab initio* molecular dynamics simulations [10] providing satisfactory rationalisation for its singular behaviour. Here, we develop a quantum theory of the solid-liquid interface, which reveals a new contribution to friction, due to the coupling of charge fluctuations in the liquid to electronic excitations in the solid. We expect that this quantum friction, which is absent in Born-Oppenheimer molecular dynamics, is the dominant friction mechanism for water on carbon-based materials. As a key result, we demonstrate a dramatic difference in quantum friction between the water-graphene and water-graphite interface, due to the coupling of water Debye collective modes with a thermally excited plasmon specific to graphite. This suggests an explanation for the radius-dependent slippage of water in carbon nanotubes [4], in terms of the nanotubes' electronic excitations. Our findings open the way to quantum engineering of hydrodynamic flows through the confining wall electronic properties.

* e-mail: nikita.kavokine@ens.fr; lyderic.bocquet@ens.fr.

While the liquid flow rate through a macroscopic channel is determined solely by its geometry, the permeability of nanoscale channels depends strongly on the amount of liquid friction at the channel walls [11]. Current theories of the solid-liquid interface picture the solid as a static external potential that acts on the fluid molecules [7], with the friction resulting from the solid's surface roughness. This approach involves a high degree of arbitrariness when applied to atomically smooth surfaces, through the choice of the molecular force fields. There is, for instance, a three order of magnitude spread in the reported molecular dynamics (MD) simulation results for the water friction coefficient inside sub-10 nm carbon nanotubes (CNTs) [12]. On the experimental side, water-carbon friction presents a particularly puzzling picture: friction is found to be much stronger on graphite [13] than on monolayer graphene [5], while in relatively large (over 30 nm in diameter) multiwall CNTs it is found to decrease with decreasing tube radius [4]. Classical MD simulations cannot account even qualitatively for this behaviour, suggesting that some key ingredients are missing from the current understanding of the solid-liquid interface. Quantum effects in the interfacial dynamics are a possible lead: a few pioneering studies have made attempts at describing electronic degrees of freedom at water-solid interfaces, through polarisable force fields [14] or Born-Oppenheimer (BO) *ab initio* molecular dynamics [10]. Yet, these still cannot capture the whole experimental picture. In this Article, we introduce a theoretical description of the solid-liquid interface that fully accounts for the quantum dynamics of the electrons in the solid. We predict that quantum effects do contribute to the solid-liquid friction, with the water-carbon interface being unique in many respects.

Single particle friction

We first consider a single point charge e moving at a height h parallel to a solid surface lying in the (x, y) plane. Taking electronic degrees of freedom into account gives rise to a polarisation charge within the solid and dissipation through the polarisation charge dynamics. We formalise this mechanism by introducing the solid surface response function $g_e(\mathbf{q}, \omega)$, defined in terms of the density-density response function χ_e :

$$g_e(\mathbf{q}, \omega) = \frac{-e^2}{4\pi\epsilon_0} \frac{2\pi}{q} \int_{-\infty}^0 dz dz' e^{q(z+z')} \chi_e(\mathbf{q}, z, z', \omega), \quad (1)$$

with the wavevector \mathbf{q} lying in the plane of the interface. Physically, $g_e(\mathbf{q}, \omega)$ relates the external potential applied to the solid in the half-space $z < 0$ to the induced potential in the half-space $z > 0$ (see Supplementary Information (SI) section 3.1). The friction force on the charge moving

at velocity \mathbf{v} then writes (SI section 1)

$$\mathbf{f} = \frac{-e^2}{8\pi^2\epsilon_0} \int d\mathbf{q} \frac{\mathbf{q}}{q} e^{-2qh} \text{Im} g_e(\mathbf{q}, \mathbf{q} \cdot \mathbf{v}). \quad (2)$$

Eq. (2) accounts for electronic friction, that is, friction through the generation of electronic excitations within the solid. This phenomenon has been invoked in various situations where classical nuclear degrees of freedom are coupled to an electron bath [15, 16]. The mechanism outlined here for a single charged particle should in principle apply as well to a dense polar liquid such as water. An electronic contribution to hydrodynamic friction, given by the sum of electronic friction forces on each water molecule, was indeed proposed in ref. [17] to account for the radius-dependent slippage in carbon nanotubes, but the prediction disagreed with experiments by orders of magnitude. The pitfall lied in the incorrect treatment of the collective excitations of the fluid, which cannot be accounted for by a sum of individual contributions.

Many-body interfacial dissipation

We account for many-body dynamics at the solid-liquid interface by building on the general framework of fluctuation-induced forces [18]. We assume for concreteness that the liquid is water, and focus on forces due to long range Coulomb interaction between the water molecules and the solid electrons. Note that we could treat similarly interactions between water and the crystal lattice. Since the dynamics of the electrons are quantum, the solid-liquid friction force is represented by an operator $\hat{\mathbf{F}}$, whose average value at time t is

$$\langle \hat{\mathbf{F}}(t) \rangle = - \int d\mathbf{r} d\mathbf{r}' \nabla_{\parallel} V(\mathbf{r} - \mathbf{r}') \langle n_w(\mathbf{r}', t) \hat{n}_e(\mathbf{r}, t) \rangle. \quad (3)$$

Here V is the Coulomb potential, n_w is the instantaneous charge density of water, \hat{n}_e is the electron density operator, and ∇_{\parallel} represents the gradient parallel to the interface; the average is over all thermal and quantum fluctuations of the system. The dynamics of water are well described within classical mechanics even at the molecular scale. Nevertheless, to ensure formal consistency, we represent the water charge density by a gaussian quantum field \hat{n}_w with prescribed correlation functions, as is done, for example, in the theory of solvation [19]. The average in Eq. (3) is then computed in the framework of many-body perturbation theory, with respect to the interaction Hamiltonian that comprises both the electron-water and electron-electron Coulomb interactions:

$$\hat{H}_{\text{int}} = \int d\mathbf{r} d\mathbf{r}' \hat{n}_w(\mathbf{r}', t) V(\mathbf{r} - \mathbf{r}') \hat{n}_e(\mathbf{r}, t) + \frac{1}{2} \int d\mathbf{r} d\mathbf{r}' \hat{n}_e(\mathbf{r}', t) V(\mathbf{r} - \mathbf{r}') \hat{n}_e(\mathbf{r}, t). \quad (4)$$

Since the system is out of equilibrium in the presence of water flow, we treat the perturbative expansion in the Schwinger-Keldysh framework [20]. After a computation reported in the SI

(section 2), our most general result is a Dyson equation relating the water-electron, water-water and electron-electron density correlation functions, whose Feynman diagram representation is given in Fig. 1d. The friction force may then be expressed in terms of the Keldysh component of the water-electron correlation function.

The formal Dyson equation can be simplified if the water and electron densities are no longer allowed to interpenetrate each other. This is a reasonable approximation as long as there is no chemisorption of water on the solid surface. The short-range Pauli repulsion effectively acts as an infinite potential barrier between the water and the electrons, as confirmed by density functional calculations of the water-graphene interface (Fig. 1b). The hydrodynamic flow profile above the solid surface is assumed to be uniform and equal to the interfacial velocity \mathbf{v} , which is justified as long as the typical range of the solid-liquid interactions is smaller than the slip length [11]. Then, expanding the Dyson equation to linear order in \mathbf{v} , we obtain a closed expression of the form $\langle \hat{\mathbf{F}} \rangle / \mathcal{A} = -\lambda \mathbf{v}$, where \mathcal{A} is the surface area, and λ is the solid-liquid friction coefficient. It separates into two terms: $\lambda = \lambda_{\text{Cl}} + \lambda_{\text{Q}}$, with

$$\lambda_{\text{Cl}} = \frac{1}{4\pi^2 k_{\text{B}} T} \int d\mathbf{q} \frac{(\mathbf{q} \cdot \mathbf{v})^2}{v^2} |V_{\text{e}}(\mathbf{q})|^2 \int_0^{+\infty} dt S_{\text{w}}(\mathbf{q}, t) \quad (5)$$

and

$$v \cdot \lambda_{\text{Q}} = \frac{1}{8\pi^2} \int_0^{+\infty} q dq (\hbar q) \int_0^{+\infty} \frac{d(\hbar\omega)}{k_{\text{B}} T} \frac{q \cdot v}{\sinh^2(\frac{\hbar\omega}{2k_{\text{B}} T})} \frac{\text{Im}[g_{\text{e}}(q, \omega)] \text{Im}[g_{\text{w}}(q, \omega)]}{|1 - g_{\text{e}}(q, \omega) g_{\text{w}}(q, \omega)|^2}. \quad (6)$$

We refer to the first contribution λ_{Cl} in Eq. (5) as the classical term, since it exactly reproduces the result obtained in the conventional surface roughness picture [7, 9]. Here, $V_{\text{e}}(\mathbf{q})$ is the average Coulomb potential acting on the interfacial water layer, and $S_{\text{w}}(\mathbf{q}, t)$ is the water charge structure factor (precise definitions of these quantities are given in the SI, section 2.5).

The second contribution λ_{Q} in Eq. (6) is absent in the roughness-based picture, and originates from the coupled water and electron dynamics, as it involves the surface response functions of both the solid and the liquid, g_{e} and g_{w} , respectively. We call it the quantum friction term. A similar term is known to arise in the non-contact friction between two dielectric media separated by a vacuum gap [18]. It is then interpreted as a dynamic analogue of the van der Waals force, here specifically derived for the solid-liquid interface under scrutiny.

Since it is accessible through MD simulations, the classical contribution has been amply studied for numerous solid-liquid systems [21]. We will therefore discuss in detail only the quantum contribution in Eq. (6), which has not been considered previously. The structure of Eq. (6) can be understood in terms of quasiparticle tunnelling between the surface fluctuation modes of the two

media, as detailed in the SI, section 2.8. Briefly, the quantum friction force $v \cdot \lambda_Q$ decomposes into a (continuous) sum over the wavevectors q of surface modes: $v \cdot \lambda_Q = (1/4\pi) \int d\mathbf{q} f_q$. The elementary friction force f_q is given by the elementary momentum $\hbar q$, multiplied by an integral over the frequencies ω , which plays the role of a tunnelling rate between modes at wavevector q . This rate is non-zero only in the presence of a water flow, which effectively increases the occupation of the liquid modes with respect to the solid modes (Fig. 1c). We note that the contribution in Eq. (6) requires thermal fluctuations, as it vanishes at 0 temperature. A purely quantum contribution to non-contact friction, that survives at 0 K, may be derived [22], but it scales as v^3 and is hence negligible for our purposes.

The quantitative evaluation of water-solid quantum friction coefficients requires both surface excitation spectra, $\text{Im} g_w(q, \omega)$ and $\text{Im} g_e(q, \omega)$, as inputs. We focus on excitations at low energy, typically below $\omega \sim 2k_B T/\hbar$ (50 meV or 10 THz), and high momenta q , since these are expected from Eq. (6) to make the dominant contributions to friction.

Water fluctuations

Our result in Eq. (6) involves the bare surface response function of water, in the absence of coupling to electronic degrees of freedom. In the frequency range under consideration, classical MD simulations are well-suited for the determination of this response functions. We have carried out such simulations for water (in the SPC/E model) in contact with graphite surfaces, for which we considered two different sets of Lennard-Jones parameters (Fig. 2a). The surface response functions were determined from the equilibrium charge correlation functions through the fluctuation-dissipation theorem, according to Eq. (1) (see SI, section 4).

We first focus on results in the long wavelength limit ($q \rightarrow 0$), displayed in Fig. 2b. The surface response function should then converge to a value determined by the bulk water dielectric permittivity $\epsilon_w(\omega)$:

$$g_w(0, \omega) = \frac{\epsilon_w(\omega) - 1}{\epsilon_w(\omega) + 1}. \quad (7)$$

It is then interpreted as an electromagnetic reflection coefficient (see SI, section 3.1). We find that this limit is essentially reached for the lowest q values accessible in our simulation ($q = 0.05 \text{ \AA}^{-1}$). Moreover, for frequencies below 100 meV, our results agree well with the long wavelength surface response function obtained from the experimentally determined $\epsilon_w(\omega)$ (see SI section 4).

Eq. (7) shows that the features in $g_w(q, \omega)$ can be analysed in terms of the well-known features of the bulk water dielectric response [23]. The low-energy surface response of water is dominated

by the Debye mode, spanning about three decades in frequency between 0.1 meV and 100 meV. It results from the collective relaxation of molecular dipoles and it is a general feature of polar liquids [24, 25]. Hence, our subsequent discussion, although focussed on water, applies qualitatively to quantum friction in other polar liquids as well. The sharp peak at around 100 meV corresponds to the water libration modes [23].

The water surface response function shows little dispersion as the momentum q is increased (Figs. 2c and S1), and only small variations are found between the two models for the graphite surfaces. At large momenta ($q \geq 1 \text{ \AA}^{-1}$), the surface response function shows an exponential decrease, which we attribute to the depletion of water near the hydrophobic surface. For the purposes of calculation, $g_w(q, \omega)$ is well represented by the sum of two Debye peaks at $\omega_{D,1} = 1.5 \text{ meV}$ and $\omega_{D,2} = 20 \text{ meV}$, with momentum-dependent oscillator strengths:

$$g_w(q, \omega) = \frac{f_1(q)}{1 - i\omega/\omega_{D,1}} + \frac{f_2(q)}{1 - i\omega/\omega_{D,2}}. \quad (8)$$

Analytical expressions for $f_1(q)$ and $f_2(q)$ are given in the SI, section 4.3; at large q , $f_1(q) + f_2(q) \propto e^{-2qd}$, with $d = 0.95 \text{ \AA}$. Further MD simulations show that the features of the water surface response relevant for quantum friction are largely unaffected by planar confinement down to 1 nm (SI section 4.4), so that the expression in Eq. (8), determined for a semi-infinite liquid, can be safely applied to nano-confined geometries.

Electronic excitations: jellium model

A solid has low energy electronic excitations if it contains free charge carriers, but the precise location of these excitations in energy-momentum space depends strongly on the exact band structure. The simplest way to account for this dependence is in the framework of the jellium model. The nuclei and core electrons are assimilated to a semi-infinite positive background, while the conduction electrons behave as free electrons (Fig. 3a). They occupy a parabolic band, $E(k) = \hbar^2 k^2 / (2m^*)$: the electronic structure is then completely determined by the effective mass m^* and the Fermi energy E_F . In general, in the jellium model, electrons are allowed to spill over the positive background edge [26]. However, in the presence of water, the spill-over is limited by the Pauli repulsion between the water and the surface electrons (Fig. 1b), so that the infinite barrier jellium model appears better suited to describing the electronic system under scrutiny. The model may then be treated within the specular reflection (SR) approximation – expressing the surface response in terms of the bulk dielectric response – with only small quantitative differences with respect to the exact semi-infinite computation (SI sections 3.2 and 5.1). A typical result for the jellium surface

response function $g_e(q, \omega)$ in the SR approximation is shown in Fig. 3b. It presents two types of features: incoherent particle-hole excitations, and a collective surface plasmon mode. We then compute the quantum friction coefficient λ_Q of water on the jellium surface according to Eq. (6), for a range of Fermi energy and effective mass values (see Fig. 3c). Note that in terms of the slip length $b = \eta/\lambda$ (with η the fluid viscosity), $\lambda = 10^5 \text{ N} \cdot \text{s} \cdot \text{m}^{-3}$ corresponds to a slip length $b = 10 \text{ nm}$ for water.

We find the quantum contribution to friction to be very small for water on semiconductor surfaces, which, for our purpose, can be described by a jellium model with low Fermi energy and effective mass. In such systems, electronic excitations are restricted to very small momenta, and we expect the hydrodynamic friction to be dominated either by the classical roughness term [7, 9] or by the optical phonon contribution (SI section 5.3). On metal surfaces, with high Fermi energy (1 - 10 eV) and effective mass close to unity, we find $\lambda_Q \sim 10^2 \text{ N} \cdot \text{s} \cdot \text{m}^{-3}$, two orders of magnitude lower than typical hydrodynamic friction coefficients, and likely smaller than the roughness-based contribution. We note that our theory does not address reactive (typically non-close-packed) metal surfaces, on which chemical bonding with water occurs. The highest values of λ_Q are obtained in the region of low Fermi energy and high effective mass. The electronic surface plasmon mode is then at low enough energy ($\sim 10 \text{ meV}$) and high enough momenta ($\sim 0.5 \text{ \AA}^{-1}$), to couple with the Debye peak of water, yielding a particular friction enhancement (Fig. 3c and S3).

The odd water-carbon interface

The classical contribution to the water-carbon friction has been extensively studied in the framework of MD simulations. On flat graphite surfaces, simulated friction coefficient values $\lambda_{\text{Cl}} \approx 10^4 - 10^5 \text{ N} \cdot \text{s} \cdot \text{m}^{-3}$ have been reported, depending on the chosen force field [27]. In carbon nanotubes, these values were found to be unaffected by wall curvature for tube radii larger than 10 nm [8, 9]. This strongly suggests that the radius-dependence of water slippage observed experimentally in carbon nanotubes with radii between 15 and 50 nm [4] cannot be explained by the classical contribution to friction alone. The experiments in ref. [4] then set an upper bound for the water-carbon classical friction at the lowest total friction coefficient measured in large radius nanotubes, that is $\lambda_{\text{Cl}}^{\text{max}} = 3 \times 10^3 \text{ N} \cdot \text{s} \cdot \text{m}^{-3}$. Hence, MD simulations likely overestimate the water-graphite friction coefficient by at least a factor of 3, which is typical in simulations of other water-solid systems [21].

We now consider quantum friction in various water-carbon systems. For a single graphene sheet, the surface response function can be calculated analytically (SI section 6.1). The result

is plotted in Fig. 4a, with a doping level $E_F = 0.1$ eV. Graphene is found to have low energy excitations ($\omega \lesssim 100$ meV) only at very small momenta ($q \lesssim 0.05 \text{ \AA}^{-1}$). An intra-layer plasmon mode is present, but it displays a steep square root dispersion at small momenta. The quantum contribution to the water friction coefficient, evaluated with Eq. (6), is accordingly found to be very small, below $10^0 \text{ N} \cdot \text{s} \cdot \text{m}^{-3}$, regardless of doping level. We conclude that hydrodynamic friction on monolayer graphene is dominated by the classical contribution and should therefore be very small ($\lambda \sim \lambda_{\text{Cl}}^{\text{max}}$). This is in line with recent measurements of water slippage on silica-supported graphene [5], which yielded friction coefficients as small as $4.5 \times 10^3 \text{ N} \cdot \text{s} \cdot \text{m}^{-3}$ (slip length $b \approx 200$ nm).

The situation must be different for water on multilayer graphite, which was found experimentally to exhibit much higher hydrodynamic friction: $\lambda \approx 2 \times 10^4 - 10^5 \text{ N} \cdot \text{s} \cdot \text{m}^{-3}$ on flat graphite surfaces [13, 28] and $\lambda \approx 3 \times 10^4 \text{ N} \cdot \text{s} \cdot \text{m}^{-3}$ in multiwall carbon nanotubes with large (50 nm) radius [4]. Indeed, in a staggered stack of graphene sheets (Fig. 4b), electrons acquire an extra degree of freedom compared to monolayer graphene, as they may tunnel between the sheets. In particular, the coupling between second nearest layers is associated with a bandwidth $4\gamma_2 = 40$ meV (Fig. 4b), resulting in a markedly different low energy excitation spectrum. In electron energy loss spectroscopy, graphite was found to exhibit a surface plasmon mode, polarised perpendicularly to the layers, at $\omega_{\text{P}} = 50$ meV (at 300 K), with a very flat dispersion in the measured momentum range, which was up to $q_{\text{max}} = 0.2 \text{ \AA}^{-1}$ at 300 K [29] and $q_{\text{max}} = 0.4 \text{ \AA}^{-1}$ at 600 K [30] (see Fig. 4a). We expect this low-energy plasmon of graphite to strongly interact with the water Debye mode, resulting in an enhancement of quantum friction. As a first approximation, we describe the plasmon contribution to the graphite surface response in terms of a Drude model, which is based on the semi-classical treatment of free electron dynamics [31]:

$$g_e(q, \omega) = \frac{\omega_{\text{P}}^2}{\omega_{\text{P}}^2 - \omega^2 - 2i\gamma\omega} \theta(q_{\text{max}} - q), \quad (9)$$

with $\gamma \sim 25$ meV the surface plasmon width [30], and θ the Heaviside step function. Using this expression in Eq. (6), we obtain a water quantum friction coefficient $\lambda_{\text{Q}} = 0.4 \times 10^3 \text{ N} \cdot \text{s} \cdot \text{m}^{-3}$ for $q_{\text{max}} = 0.2 \text{ \AA}^{-1}$ and $\lambda_{\text{Q}} = 5 \times 10^3 \text{ N} \cdot \text{s} \cdot \text{m}^{-3}$ for $q_{\text{max}} = 0.4 \text{ \AA}^{-1}$. This is orders of magnitude larger than the expectation for graphene (Fig. 4c), and comparable to the upper bound for the classical contribution $\lambda_{\text{Cl}}^{\text{max}}$. Hence, the Drude model estimate suggests that the quantum contribution may account for the difference in hydrodynamic slippage between monolayer graphene and multilayer graphite.

Going beyond a phenomenological treatment for the water-graphite quantum friction is par-

ticularly challenging, due to the very large unit cell required for a numerical investigation of low energy and high momentum surface excitations [32]. We propose here a simplified microscopic model to extract the essential physics at play. Our starting point is that the free charge carriers contributing to the low energy plasmon are located mainly on the B sublattice [33] (Fig. 4b). The flat plasmon dispersion has been attributed to the shape of the bands containing those free carriers [30]. As a consequence of interlayer coupling, these are nearly flat up to parallel momentum $k \sim \gamma_1/v_F = 0.06-0.11 \text{ \AA}^{-1}$, with γ_1 the nearest-neighbour interlayer coupling parameter (Fig. 4b) and v_F the graphene Fermi velocity. Then, from the perspective of low-energy excitations, graphite may be pictured as an array of independent 1D chains extending perpendicular to the layers, at least within a certain momentum range. This assembly of localised oscillators is then expected to have excitations whose energy does not depend on wavevector, as observed experimentally.

Following this idea, we consider only the atoms on the B sublattice, which form an assembly of tight-binding chains with coupling parameter $\gamma_2 = 10 \text{ meV}$. At sufficiently large momenta ($q \gtrsim 1/(2c) = 0.14 \text{ \AA}^{-1}$, with $c = 3.35 \text{ \AA}$ the interlayer spacing), we may consider that the external field acts only on the topmost (surface) atoms. We then compute the local density response of the topmost atom a of a 1D chain $\delta n_a(q, \omega) = \chi_a(q, \omega)\phi_a(q, \omega)$, where ϕ_a is the potential acting on atom a (see SI section 6.2). Then, treating the Coulomb interactions between the chains in the random phase approximation, we obtain the graphite surface response function as

$$g_e(q, \omega) = \frac{n_s v_q \chi_a(q, \omega)}{n_s v_q \chi_a(q, \omega) - 1}, \quad (10)$$

where $v_q = \frac{e^2}{4\pi\epsilon_0} \frac{2\pi}{q}$ is the 2D Coulomb potential and n_s is the density of charge carriers contributing to the low energy mode. Our simple model accounts indeed for an excitation continuum around $\omega = 40 \text{ meV}$, whose intensity slowly decays with momentum (Fig. S5). An estimate for the parameter n_s is provided by the free charge carrier density in bulk graphite at 300 K ($n_s = 2.3 \times 10^{12} \text{ cm}^{-2}$, see SI section 6.2): this yields a friction coefficient $\lambda_Q = 1.8 \times 10^4 \text{ N}\cdot\text{s}\cdot\text{m}^{-3}$, slightly larger than the Drude model estimates, and within the range of experimentally measured water friction coefficients on graphite (Fig. 4d). Ultimately, the value of n_s depends on the details of the electronic structure at the graphite surface, which undergoes renormalisation in the presence of water. An increase in the density of states at low energy and high momenta due to electron scattering on water fluctuations may lead to a higher apparent n_s (the upper limit being the total electron density on the B sublattice, $4.3 \times 10^{14} \text{ cm}^{-2}$) and to a further increase in the expected value for the quantum friction coefficient (Fig. 4c).

Overall, our theory predicts a strong difference in quantum friction between monolayer and

multilayer carbon structures, explaining how water can exhibit larger slippage on monolayer graphene [5] than on multilayer graphite [4, 13, 28]. This further suggests an explanation for the radius-dependent water slippage in multiwall carbon nanotubes [4]. In these quite large nanotubes (15 – 50 nm radius), while the water surface response is unaffected by confinement (SI section 4), the interlayer coupling is known to strongly depend on radius. It was observed that a 50 nm radius tube has locally a graphite-like structure, while in a 10 nm radius tube the shells are completely decoupled [34]. Therefore, in large radius nanotubes, water is subject to graphite-like high quantum friction, while in smaller radius nanotubes water experiences graphene-like low friction, likely dominated by the classical contribution.

The quantitative relevance of this argument can be checked, at the simplest level, in the framework of the Franklin model [35, 36], which relates the probability p of two layers being misaligned in a graphite structure to the average interlayer spacing d : $d = 3.44 - 0.086 \cdot (1 - p^2)$ (Å). The dependence of d on the inner radius R for a multiwall nanotube can be inferred from experiment [34] (see SI section 6.4). We may then assume that the electron density n_s in Eq. (10) scales according to $n_s(R) = n_s^0(1 - p(R))$, and we choose $n_s^0 = 10^{13} \text{ cm}^{-2}$ so that $\lambda(R \rightarrow \infty) = 4.4 \times 10^4 \text{ N} \cdot \text{s} \cdot \text{m}^{-3}$. The resulting prediction for the slip length is shown in Fig. 4d, and is found to be in good agreement with the experimental data. We note that if the inner shell tubes are semiconducting, the radius-dependent band gap $E_g(R) = (2/3)v_F/R$ [37] may also reduce the number of charge carriers contributing to low energy excitations: we then expect a scaling $n_s(R) = n_s^0 e^{-E_g(R)/k_B T}$, which also provides reasonable agreement with the data (Fig. 4d). While the details of electronic excitations in multiwall carbon nanotubes are hard to investigate theoretically, our theory strongly suggests that quantum friction is a key ingredient for determining the water slip length in these systems.

Perspectives

Our theory predicts quantum effects in the dynamics of the solid-liquid interface. We show that hydrodynamic friction results not only from the static roughness of the solid surface, but also from the coupling of water fluctuations to electronic excitations within the solid. Such “quantum friction” is uniquely revealed at the water-carbon interface. Water friction is not anomalously low on graphene, it is rather anomalously high on graphite, due to the quantum contribution resulting from a graphite-specific terahertz plasmon mode. This finding enables us to rationalise the peculiar friction properties of water on carbon surfaces, and in particular the radius dependence of slippage in carbon nanotubes. More generally, quantum friction may be an important contribution to hydrodynamic friction on atomically smooth surfaces, provided that these have electronic exci-

tations at low energy ($\omega \lesssim 100$ meV) and high momenta ($q \sim 0.5 \text{ \AA}^{-1}$), which may couple to the Debye mode of water. However, true atomic smoothness cannot be achieved for any material, since many surfaces become oxidised or charged in water. For instance, the negligible water slippage observed on hexagonal boron nitride surfaces [4] can be attributed to the chemisorption of charged species [11, 38]. We stress that quantum friction is an effect beyond the BO approximation. While it can be overcome in the numerical treatment of single molecules on surfaces [16], the BO approximation remains a fundamental limitation in simulations of solid-liquid interfaces. Our results call for the development of new methods for simulating such complex interfacial systems [39].

-
- [1] Bocquet, L. Nanofluidics coming of age. *Nat. Mater.* **19**, 254–256 (2020).
- [2] Holt, J. K. *et al.* Fast Mass Transport Through Sub-2-Nanometer Carbon Nanotubes. *Science* **312**, 1034–1037 (2006).
- [3] Whitby, M., Cagnon, L., Thanou, M. & Quirke, N. Enhanced fluid flow through nanoscale carbon pipes. *Nano letters* **8**, 2632–2637 (2008).
- [4] Secchi, E. *et al.* Massive radius-dependent flow slippage in carbon nanotubes. *Nature* **537**, 210–213 (2016).
- [5] Xie, Q. *et al.* Fast water transport in graphene nanofluidic channels. *Nat. Nanotech.* **13**, 238–245 (2018).
- [6] Faucher, S. *et al.* Critical Knowledge Gaps in Mass Transport through Single-Digit Nanopores: A Review and Perspective. *J. Phys. Chem. C* **123**, 21309–21326 (2019).
- [7] Bocquet, L. & Barrat, J. L. Flow boundary conditions from nano- to micro-scales. *Soft Matter* **3**, 685–693 (2007).
- [8] Thomas, J. A. & McGaughey, A. J. Reassessing fast water transport through carbon nanotubes. *Nano Lett.* **8**, 2788–2793 (2008).
- [9] Falk, K., Sedlmeier, F., Joly, L., Netz, R. R. & Bocquet, L. Molecular origin of fast water transport in carbon nanotube membranes: Superlubricity versus curvature dependent friction. *Nano Lett.* **10**, 4067–4073 (2010).
- [10] Tocci, G., Joly, L. & Michaelides, A. Friction of water on graphene and hexagonal boron nitride from Ab initio methods: Very different slippage despite very similar interface structures. *Nano Lett.* **14**, 6872–6877 (2014).
- [11] Kavokine, N., Netz, R. R. & Bocquet, L. Fluids at the Nanoscale: From Continuum to Subcontinuum Transport. *Annu. Rev. Fluid Mech.* **53** (2021).
- [12] Sam, A. *et al.* Fast transport of water in carbon nanotubes: a review of current accomplishments and challenges. *Molecular Simulation* 1–20 (2020).

- [13] Maali, A., Cohen-Bouhacina, T. & Kellay, H. Measurement of the slip length of water flow on graphite surface. *Appl. Phys. Lett.* **92**, 2007–2009 (2008).
- [14] Misra, R. P. & Blankschtein, D. Insights on the Role of Many-Body Polarization Effects in the Wetting of Graphitic Surfaces by Water. *J. Phys. Chem. C* **121**, 28166–28179 (2017).
- [15] Wodtke, A. M., Tully, J. C. & Auerbach, D. J. Electronically non-adiabatic interactions of molecules at metal surfaces: Can we trust the Born-Oppenheimer approximation for surface chemistry? *Int. Rev. Phys. Chem.* **23**, 513–539 (2004).
- [16] Dou, W. & Subotnik, J. E. Perspective: How to understand electronic friction. *J. Chem. Phys.* **148** (2018).
- [17] Sokoloff, J. B. Enhancement of the water flow velocity through carbon nanotubes resulting from the radius dependence of the friction due to electron excitations. *Phys. Rev. E* **97**, 33107 (2018).
- [18] Volokitin, A. I. & Persson, B. N. Near-field radiative heat transfer and noncontact friction. *Rev. Mod. Phys.* **79**, 1291–1329 (2007).
- [19] Song, X., Chandler, D. & Marcus, R. A. Gaussian field model of dielectric solvation dynamics. *J. Phys. Chem.* **100**, 11954–11959 (1996).
- [20] Rammer, J. & Smith, H. Quantum field-theoretical methods in transport theory of metals. *Rev. Mod. Phys.* **58**, 323–359 (1986).
- [21] Bocquet, L. & Charlaix, E. Nanofluidics, from bulk to interfaces. *Chem. Soc. Rev.* **39**, 1073–1095 (2010).
- [22] Pendry, J. B. Shearing the vacuum - Quantum friction. *J. Phys. Condens. Matter* **9**, 10301–10320 (1997).
- [23] Carlson, S., Brünig, F. N., Loche, P., Bonthuis, D. J. & Netz, R. R. Exploring the Absorption Spectrum of Simulated Water from MHz to Infrared. *J. Phys. Chem. A* **124**, 5599–5605 (2020).
- [24] Sato, T. & Buchner, R. Dielectric relaxation processes in ethanol/water mixtures. *J. Phys. Chem. A* **108**, 5007–5015 (2004).
- [25] Koeberg, M., Wu, C. C., Kim, D. & Bonn, M. THz dielectric relaxation of ionic liquid:water mixtures. *Chem. Phys. Lett.* **439**, 60–64 (2007).
- [26] Lang, N. D. & Kohn, W. Theory of metal surfaces: Charge density and surface energy. *Phys. Rev. B* **1**, 4555–4568 (1970).
- [27] Paniagua-Guerra, L. E., Gonzalez-Valle, C. U. & Ramos-Alvarado, B. Effects of the Interfacial Modeling Approach on Equilibrium Calculations of Slip Length for Nanoconfined Water in Carbon Slits. *Langmuir* **36**, 14772–14781 (2020).
- [28] Radha, B. *et al.* Molecular transport through capillaries made with atomic-scale precision. *Nature* **538**, 222–225 (2016).
- [29] Portail, M., Carrere, M. & Layet, J. M. Dynamical properties of graphite and peculiar behaviour of the low-energy plasmon. *Surf. Sci.* **433**, 863–867 (1999).
- [30] Laitenberger, P. & Palmer, R. E. Plasmon dispersion and damping at the surface of a semimetal. *Phys.*

- Rev. Lett.* **76**, 1952–1955 (1996).
- [31] Pitarke, J. M., Silkin, V. M., Chulkov, E. V. & Echenique, P. M. Theory of surface plasmons and surface-plasmon polaritons. *Reports Prog. Phys.* **70**, 1–87 (2007).
- [32] Lavor, I. R., Cavalcante, L. S. R., Chaves, A., Peeters, F. M. & Van Duppen, B. Probing the structure and composition of van der Waals heterostructures using the nonlocality of Dirac plasmons in the terahertz regime. *2D Mater.* **8**, 015014 (2020).
- [33] Tománek, D. *et al.* Theory and observation of highly asymmetric atomic structure in scanning-tunneling-microscopy images of graphite. *Phys. Rev. B* **35**, 7790–7793 (1987).
- [34] Endo, M. *et al.* Stacking nature of graphene layers in carbon nanotubes and nanofibres. *J. Phys. Chem. Solids* **58**, 1707–1712 (1997).
- [35] Franklin, R. E. The structure of graphitic carbons. *Acta Crystallogr.* **4**, 253–261 (1951).
- [36] Speck, J. S., Endo, M. & Dresselhaus, M. S. Structure and intercalation of thin benzene derived carbon fibers. *J. Cryst. Growth* **94**, 834–848 (1989).
- [37] Charlier, J. C., Blase, X. & Roche, S. Electronic and transport properties of nanotubes. *Rev. Mod. Phys.* **79**, 677–732 (2007).
- [38] Xie, Y., Fu, L., Niehaus, T. & Joly, L. Liquid-Solid Slip on Charged Walls: The Dramatic Impact of Charge Distribution. *Phys. Rev. Lett.* **125**, 1–7 (2020).
- [39] Pham, T. A., Ping, Y. & Galli, G. Modelling heterogeneous interfaces for solar water splitting. *Nat. Mater.* **16**, 401–408 (2017).

Figure 1. Theory of solid-liquid quantum friction. **a.** Artist’s view of the quantum friction phenomenon: water charge fluctuations couple to electronic excitations within the solid surface, represented by the orange arrow. **b.** Average electronic density, as obtained from density functional calculations (SI, section 7), at the water-graphene interface. **c.** Schematic of the quantum friction mechanism, showing quasiparticle tunnelling between two surface modes at wavevector \mathbf{q} and frequency $\omega_{\mathbf{q}}$. The filling of the blue parabolas represents the occupation of each mode, according to the Bose-Einstein distribution n_B . The back and forth tunnelling rates γ are different in the presence of flow, resulting in net momentum transfer from the liquid to the solid. Further details are given in the SI, section 2.8. **d.** Feynman diagram representation of the Dyson equation for the electron-water density correlation function. Full lines are electron propagators, and dashed lines are water propagators. The equation expresses that electron-water correlations are mediated by all possible coupled fluctuations of the water and electron densities.

Figure 2. Surface dielectric response of water. **a.** Snapshot of the MD simulation used for determining the water surface response function. The graphene supercell size is $128 \times 123 \text{ \AA}^2$. **b.** Surface response function g_w of water versus frequency, in the long wavelength limit ($q \rightarrow 0$). The various curves correspond to results obtained from MD simulations of the water-graphite interface with two different sets of molecular parameters (named ‘Aluru’ and ‘Werder’, see text), and to the $q = 0$ prediction of Eq. (7), obtained from the experimental and simulated bulk dielectric constant. All the determinations of the surface response function agree well in the long wavelength limit. **c.** Surface response function of water in energy-momentum space, as obtained by fitting the simulation data with two Debye peaks (Eq. (8)).

Figure 3. Quantum friction of water on a jellium surface. **a.** Schematic of the infinite barrier jellium model: the water and solid electrons are separated by an infinite potential barrier. **b.** Surface response function for a semi-infinite jellium (electron density parameter $r_s = 5$) in energy-momentum space. **c.** Quantum friction coefficient for water on a jellium surface, as a function of the jellium Fermi energy and effective mass (in units of electron mass).

Figure 4. Quantum friction at the water-carbon interface. **a.** Surface response function of doped graphene ($E_F = 0.1 \text{ eV}$) in energy-momentum space, and experimental data [29, 30] for the graphite surface plasmon mode. **b.** Schematic of the electron movement corresponding to the graphite surface plasmon, and definition of the interlayer coupling parameters. **c.** Quantum friction coefficient for water on graphene and graphite as a function of charge carrier density. For

graphene, the carrier density is determined by the doping level. For graphite, the friction coefficient is determined from the 1D chain model (Eq. (10)), where the carrier density corresponds to the parameter n_s . **d.** Water slip length ($b = \eta/\lambda$, with η the water viscosity) in multiwall carbon nanotube as a function of inner tube radius. The green symbols are experimental data from refs. [3, 4, 13], and the full lines are theoretical predictions, corresponding to different models for the radius dependence of n_s in Eq. (10). The error bars correspond to the experimental uncertainty, which has been estimated in ref. [4].

Acknowledgements

The authors thank A. Robert for help with molecular dynamics simulations, and acknowledge fruitful discussions with A. Robert, B. Douçot, R. Netz, B. Coasne, N. Lorente, and B. Rotenberg. L.B. acknowledges funding from the EU H2020 Framework Programme/ERC Advanced Grant agreement number 785911-Shadoks and ANR project Neptune. This work has received the support of "Institut Pierre-Gilles de Gennes", program ANR-10-IDEX-0001-02 PSL and ANR-10-LABX-31. The authors acknowledge the French HPC resources of GENCI for the grant A9-A0070807364. The Flatiron Institute is a division of the Simons Foundation. L.B. and M.-L.B. dedicate this article to the memory of Jorge Iribas Cerdá.

Data availability

The molecular dynamics simulation data (Fig. 2, S1, S2) are available on Zenodo (doi:10.5281/zenodo.5242930). The rest of the data are included with the paper.

Author contributions

L.B., M.-L.B. and N.K. conceived the project. N.K. developed the theoretical framework. N.K. and L.B. co-wrote the paper, with inputs from M.-L.B. All authors discussed the results and commented on the manuscript.

Competing interests

The authors declare no competing interests.

Correspondence and requests for materials

should be addressed to N.K. or L.B.

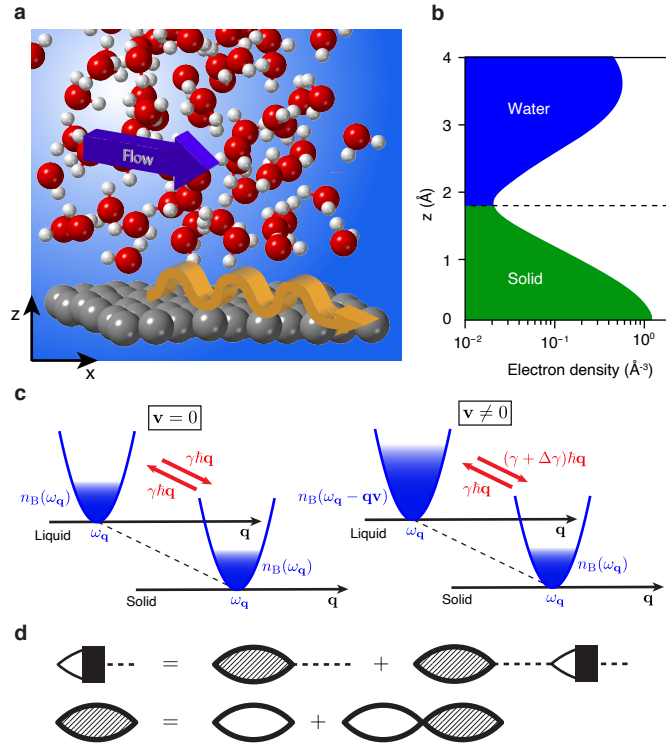


FIG. 1.

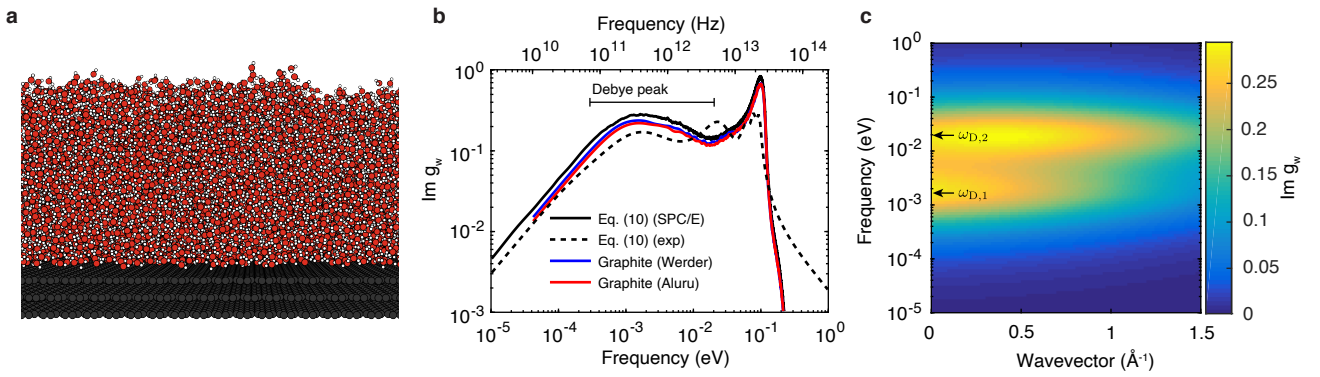


FIG. 2.

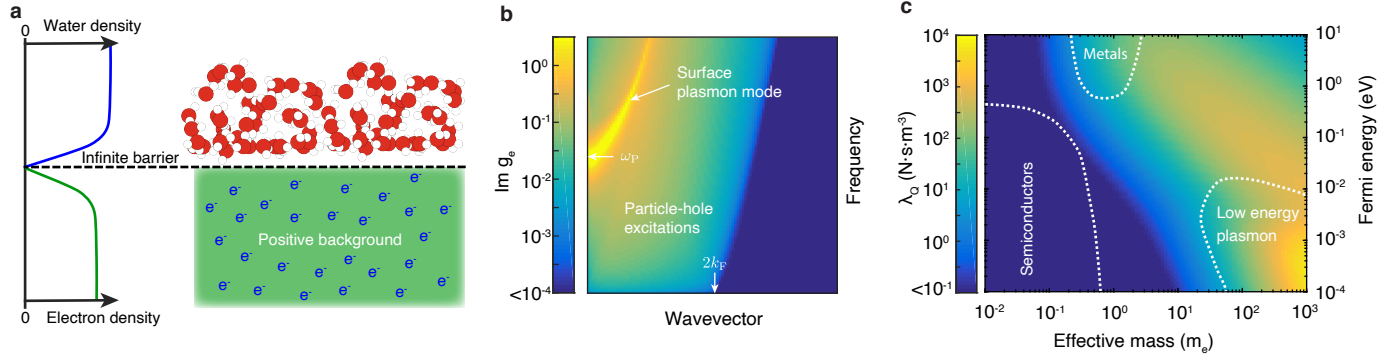


FIG. 3.

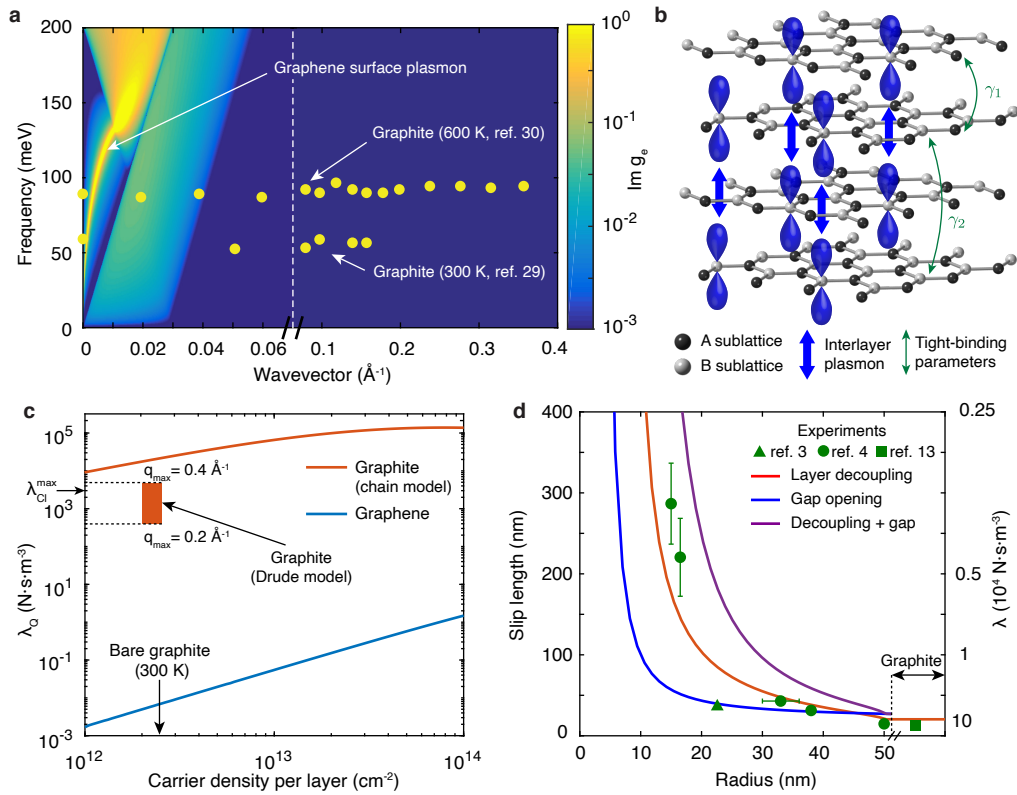


FIG. 4.